Crystallographic Studies on the Complex Behavior of Nicotine Binding to P450cam (CYP101)

7 AUTHORS, INCLUDING:

Laura M Shireman
University of Washington Seattle
10 PUBLICATIONS **165** CITATIONS

Donald S. Matteson
Washington State University
206 PUBLICATIONS **4,920** CITATIONS

Jeffrey P Jones
Washington State University
111 PUBLICATIONS **3,355** CITATIONS

Crystallographic Studies on the Complex Behavior of Nicotine Binding to P450cam (CYP101)[†]

Michael Strickler,[§] Barry M. Goldstein,[§] Kathleen Maxfield,[‡] Laura Shireman,[‡] Gyungyoun Kim,[‡] Donald S. Matteson,[‡] and Jeffrey P. Jones*,[‡]

Department of Biophysics, University of Rochester, Rochester, New York 14627, and Department of Chemistry, Washington State University, Pullman, Washington 99164-4630

Received May 20, 2003; Revised Manuscript Received August 8, 2003

ABSTRACT: Crystallographic and spectroscopic studies have been undertaken to characterize the binding behavior of the non-native substrate nicotine in the active site of the monooxygenase hemoprotein cytochrome P450cam. Despite the existence of a theoretical model that is consistent with the observed distribution of monooxygenation products, the crystal structure of the complex indicates that the primary binding mode of nicotine is unproductive. The structure is confirmed by spectral data that indicate direct coordination of substrate pyridine nitrogen with the heme iron. This would be the proper structure for evaluating binding affinity and inhibition. Reduction of the heme from Fe(III) to Fe(II) and introduction of carbon monoxide into crystals of the nicotine−P450cam complex, to simulate molecular oxygen binding, produces reorientation of the nicotine. This orientation is the appropriate one for predicting regioselectivity and the kinetic features of substrate oxidation. While it is not clear that such complicated behavior will be exhibited for other enzyme−substrate interactions, it is clear that a single crystal structure for a given substrate−enzyme interaction may not provide a good description of the binding mode responsible for product formation.

Crystal structures have been available for P450 enzymes for almost 20 years. Numerous studies have been done to predict the binding affinity and important features of the bacterial P450 enzymes (*1−11*). More recently, structures have become available for mammalian enzymes (*12*, *13*). The P450 family is rather unique among enzymes in its ability to bind compounds of widely varying structure in the same active site. These enzymes can also give multiple products that must arise from multiple binding modes for the same compound. Given this diversity of binding modes, it remains to be seen how valuable a single crystal structure will be in drug design. Herein we describe the multiple binding modes that are available to a single substrate throughout the catalytic cycle for P450cam, a P450 enzyme with a cornucopia of structural information.

To best perform rational modeling of the binding of novel substrates to enzymes, experimental structural information is needed. The structure of cytochrome P450cam with its natural substrate (*R*)-camphor bound has previously been determined to a resolution of 1.63 Å (*14*). Crystal structures have also been determined for the substrate-free enzyme, for the binding of camphor-like substrate analogues (*15*), and

for the inhibitors metyrapone and phenylimidazole (*16*). Structures with carbon monoxide bound have been used as an analogue for molecular oxygen in the crystallographic study of the oxygen-binding step in the P450 reaction pathway (*17*). Many of the crucial residues for P450cam action have also been studied by mutagenesis (*18*). The mutagenesis studies have underscored the importance of tyrosine 96 in camphor binding; the hydrogen bond between tyrosine 96 and camphor observed in the crystal structure is important for camphor metabolism. It was subsequently discovered that substrates for cytochrome P450cam need not be similar to camphor; indeed, many mammalian P450 substrates are also P450cam substrates (*19*).

One such mammalian substrate is nicotine, or 3-(2-(*N*-methylpyrrolidinyl))pyridine (*10*). As the name indicates, nicotine is composed of a pyridine ring joined to *N*-methylpyrrolidine by a carbon−carbon single bond. Binding, labeling, and kinetic studies have been performed on the metabolism of nicotine by P450cam as well as for mammalian enzymes (*10*, *20−22*); these have indicated that nicotine is hydroxylated by P450cam with high regiospecificity, and that there are differences in binding and kinetics between the enantiomers. Molecular dynamics simulations and calculations of free energy differences were performed for the binding of (*R*)- and (*S*)-nicotine to the active site of P450cam (*10*). These simulations were able to predict the binding free energy difference between (*R*)-nicotine and its enantiomer (*S*)-nicotine, as experimentally determined by spectral dissociation constants, and resulted in the configuration shown in Figure 1.
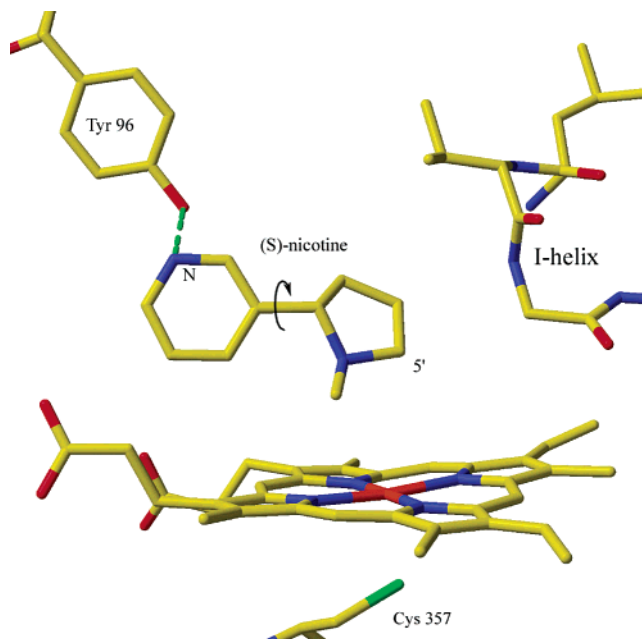
FIGURE 1: Schematic figure derived from the theoretical orientation of (S)-nicotine in the P450cam active site. The arrow indicates the rotational freedom of the pyrrolidine moiety. A hydrogen bond is shown between Tyr 96 and the nicotine pyridine nitrogen, from analogy with the binding of the native substrate camphor. The 5′ carbon that is the primary site of hydroxylation is indicated.

Experimental labeling studies have shown that hydroxylation occurs primarily at the 5′ cis and trans positions on the pyrrolidine ring, both of which lead to identical iminium ion product (*21*); a small fraction of hydroxylation also occurs on the pyrrolidine methyl group. The simulation resulted in catalytic binding modes consistent with formation of these products for (S)-nicotine. The conformation is similar to that shown in Figure 1; however, this figure does not show the oxygen bond to iron. With all starting configurations, the pyrrolidine ring was moved into proximity to the heme iron−oxene, to allow for hydroxylation at the experimentally determined sites. The pyridine nitrogen was hydrogen bonded to tyrosine 96, by analogy with camphor binding. Rotation about the bond between the pyridine and pyrrolidine would presumably allow for either cis or trans 5′ hydroxylation, although experimental data indicate that this rotation is slow relative to the forward rate of catalysis (*10, 20*). Finally, these results are in conflict with the known preference for type II binding, in that the pyrrolidine nitrogen is sterically hindered, and pyridine might be expected to coordinate more strongly with the heme iron (*23, 23*).

To determine which nitrogen of nicotine was coordinated to the heme, an analogue of nicotine with a phenyl ring in place of the pyridine ring, 2-(*N*-methylpyrrolidinyl)benzene, was synthesized, and the differences in the energetics of binding to the ground state by nicotine and 2-(*N*-methylpyrrolidinyl)benzene were assessed. These studies led to a model for binding of nicotine in which the pyridine nitrogen coordinates more tightly to the iron, while the pyrrolidine nitrogen can coordinate but with a much lower affinity.

Finally, crystallographic studies were undertaken to test the above computer model for (S)-nicotine and to explore the features of the binding site that distinguish between nicotine and the phenylimidazoles. In addition, nicotine binding was studied in the presence of carbon monoxide in

order to mimic the structure of the difficult-to-observe (*24*) oxygen-bound intermediate in the catalytic cycle (*17*).

EXPERIMENTAL METHODS

All fine chemicals were purchased from Aldrich (Milwaukee, WI). Deuterated solvents were purchased from Cambridge Isotope Laboratories, Inc. (Andover, MA). Site-directed mutagenesis was performed with the Quick Change Site-Directed Mutagenesis Kit from Stratagene (La Jolla, CA). All solvents were purchased from J. T. Baker, Inc. (Phillipsburg, NJ). Site-directed mutagenesis was confirmed by sequencing using an Applied Biosystems 373 DNA sequencer (Foster City, CA).

Synthesis of (S)-N-Methyl-2-phenylpyrrolidine. (S)-2-Phenylpyrrolidine (*34*) was treated with 37% formaldehyde and sodium cyanoborohydride in methanol at 0 °C, resulting in the title compound in 83% yield. ^{1}H NMR (300 MHz, CDCl$_3$): δ 1.8 (m, 2H), 1.9 (m, 1H), 2.1 (s, 3H), 2.15 (m, 2 H), 3.0 (t, 1H), 3.3 (t, 1H), 7.3−7.4 (m, 5H).

Binding Spectra Measurements. Binding spectra were determined with an Aminco DW-2000 dual-beam spectrophotometer. A solution of P450cam (6 μM) in Tris buffer (pH 7.4 at 30 °C) was split between two matched quartz cuvettes. The sample chamber was maintained at 30 °C. The difference spectra between the sample and reference cells were recorded between 350 and 450 nM. The absorption difference between the peak and the trough absorbance with increasing concentration was fit to the equation for a hyperbola as described previously (*35*).

Protein Expression, Purification, and Crystallization. Cytochrome P450cam, modified to incorporate a six-histidine tag at the C-terminus, was expressed and purified as described by French et al. (*25*), followed by exchange of the resultant partially purified protein into 50 mM Tris buffer, pH 7.4, using a pre-equilibrated Sephadex G-25 M column (Amersham Pharmacia). The protein was then subjected to strong anion-exchange chromatography using the PerSeptive Biosystems BioCAD Sprint system (PE Biosystems). The anion-exchange purification was accomplished using 20 mM Tris buffer, pH 7.4, with a gradient of 0−1 M NaCl. The sample was exchanged at 4 °C against a YM-30 membrane in the Amicon ultrafiltration cell into pH 7.0 buffer containing 50 mM KP$_i$, 250 mM KCl, 1 mM DTT, and 1 mM (S)-nicotine. The sample was then concentrated under pressurized argon in the ultrafiltration cell to a final concentration of 20−30 mg/mL.

Although protocols for producing orthorhombic crystals were provided in the literature (*26*), in our hands these conditions did not produce crystals. Instead, sitting-drop vapor diffusion was discovered to yield crystals. Crystals of P450cam were grown at 4 °C in a 24-well tissue-culture plate from a reservoir solution of the above buffer plus 16−24% w/v poly(ethylene glycol), molecular weight 8000. Each sitting drop, placed on a microbridge in each reservoir, contained 2 μL of 20−30 mg/mL protein and 2 μL of reservoir solution. The setup was performed at 4 °C with streaming argon introduced to reduce potential oxidation. Red bipyramidal crystals of irregular appearance and approximately 0.3 mm in their largest dimension appeared in several of the wells after 1−2 days.

Data Collection and Processing. Crystals were soaked for ∼1 h at 4 °C in a pH 7.0 cryoprotectant solution containing

Table 1: Data Collection and Refinement Statistics for Nicotine−P450cam Complexes

	A	B
data set	1	2
crystal	cam + nicotine	cam + nicotine + CO(?)
complex	CHESS	University of Rochester
location		
crystal system	tetragonal	tetragonal
space group	$P4_32_12$	$P4_32_12$
$a = b$ (Å)	64.05	63.46
c (Å)	251.06	248.76
resolution (d_{min}, Å)	2.30	2.85
no. of unique reflections	21616	10395
data completeness (%) (overall)	86.0	80.9
(at d_{min})	56.4	70.1
R_{sym} (%)[a] (overall)	6.6	7.5
(at d_{min})	24.2	39.2
$\langle I \rangle/\sigma(I)$ (overall)	12.4	12.4
(at d_{min})	4.0	2.0
reflections ($|F| > 0$)	20892	10025
protein atoms in asymmmetric unit	3271	3271
no. of ordered solvent molecules	122	25
R_{cryst} (%)[b]	22.3	23.8
R_{free} (%)	26.4	28.4
RMS bond length (Å)	0.009	0.011
RMS angle (deg)	1.439	1.482
RMS dihedral angle (deg)	23.066	22.986
RMS improper angle (deg)	1.428	1.192

[a] $R_{sym} = \sum |I - \langle I \rangle|/\sum I$, where I is an individual reflection and $\langle I \rangle$ is the mean for symmetry-related reflections. [b] $R_{cryst} = \sum ||F_o| - |F_c||/\sum |F_o|$, where F_o and F_c are observed and calculated structure factors, respectively.

50 mM KP$_i$, 250 mM KCl, 1 mM DTT, 1 mM (*S*)-nicotine, and 30% PEG 400. In the case of the CO-exposed complex, the crystal was then transferred for several minutes to a sealed CO-bubbled drop of the above cryoprotectant with the reducing agent dithionite added. The method previously used to determine a CO-bound structure (*17*) requires use of capillaries under positive CO pressure, which is not feasible for cryocrystallography (*27*). For data collection, all crystals were mounted in nylon loops (Hampton Research) and flash cooled to −170 °C in a dry nitrogen stream (Molecular Structure Corp.).

As will be described, two X-ray diffraction data sets were collected on two different crystals. Data for the P450cam−nicotine complex from the first crystal (data set A) were collected at the A-1 station at CHESS using a 2K × 2K ADSC charge-coupled detector (*28*). Data for a CO-exposed P450cam−nicotine complex from the second crystal (data set B) were collected at the University of Rochester using a R-AXIS II imaging plate system and Cu Kα radiation produced by a Rigaku rotation anode RU200 operated at 50 kV and 100 mA (Molecular Structure Corp.). All indexing and scaling were carried out using the HKL software package (*29*). Data processing statistics are summarized in Table 1.

Data Refinement. The data were provided with starting model phases from coordinates for an isomorphous tetragonal form of P450cam, kindly provided by Dr. Ilme Schlichting, EMBL Heidelberg. Refinement of data set A was initially performed with X-PLOR (Brünger, 1992 no. 5), while further refinements of data set A, and all refinement of data set B, were performed using CNS (*30*) with maximum-likelihood methodology (*31*). Topology and parameter files required by X-PLOR and CNS to characterize the (*S*)-nicotine model were generated using the utility XPLO2D (*32*).

For data set A, rigid-body and conjugate-gradient minimization refinements were followed by Cartesian-simulated annealing with the binding site harmonically constrained by means of a nicotine model that was omitted from refinement. This produced $F_o - F_c$ and $2F_o - F_c$ electron-density-simulated annealing omit maps with a well-defined bilobed region of density into which the (*S*)-nicotine substrate could be fitted. The pucker of the nicotine pyrrolidine ring was restrained to the pucker observed in the crystal structure of nicotine from the Cambridge Structural Database; this provided the best density fit out of those modified nicotine compounds in the database that were examined. Initial conjugate-gradient and Cartesian-simulated annealing refinement with substrate model included were performed using X-PLOR, whereupon maximum likelihood refinement using CNS was adopted. All positive reflections were included, and bulk solvation and overall anisotropic *B*-factor refinement were applied at each step. Additional conjugate-gradient and torsional annealing, which imposes torsion angle restraints on simulated annealing, further reduced R_{free} and R. Solvent molecules were then added on the basis of peak height and stereochemistry by means of the X-SOLVATE water search module from QUANTA 97 (Molecular Simulations Inc.). Additionally, it became possible, using the X-BUILD module of QUANTA 97, to fit the last two residues of the native protein C-terminus as well as the first two histidines of the six-histidine C-terminus tag. This was followed by further cycles of torsion angle annealing with waters fixed, conjugate-gradient refinement, and grouped *B*-factor refinement. The van der Waals radii of the nicotine pyridine nitrogen, the axial cysteine thiolate sulfur, and the heme iron were set to zero throughout refinement to allow the observed density to dictate the substrate position. Weak harmonic bonds were imposed and released to determine the correct pyridine nitrogen−heme iron and cysteine sulfur−heme iron coordination distances.

The refinement of data set B proceeded similarly, using the refined model from the previous data set with the nicotine removed. Following rigid-body refinement, the data were

subjected to maximum-likelihood Cartesian-simulated annealing with a nicotine model used to harmonically restrain the binding site, but omitted from the refinement calculation. A new nicotine model was fitted into the resulting $F_o - F_c$ and $2F_o - F_c$ simulated annealing omit maps, which were calculated with σA weighting to further reduce map bias from the model. The data set collected at the University of Rochester on the CO-exposed crystal had too high a ratio of free model parameters to data to be amenable to Cartesian-simulated annealing refinement. Thus, torsional-simulated annealing was employed on models with fitted substrate, followed by individual temperature factor refinement, in which temperature factors were grouped as main chain, side chains, heme, and nicotine. Hydration of the refined model was performed using the program XtalView (*33*), and the result was subjected to individual temperature factor refinement. Refinement statistics are summarized in Table 1.

RESULTS

Binding Spectra. Binding constants for (*S*)-nicotine and (*S*)-*N*-methyl-2-phenylpyrrolidine were determine by titration of P450cam with the appropriate substrate, as described previously (*35*). (*S*)-Nicotine was found to bind with a K_s value of 10 ± 3 μM, and to give a type II spectrum (vide infra). (*S*)-*N*-Methyl-2-phenylpyrrolidine was found to bind with a K_s value of 2500 ± 200 μM, and to also give a type II spectrum. The magnitude of the difference in absorption was the same for both compounds at saturation.

Data Set A: Nicotine−P450cam Complex. The overall structure of P450cam, including its active-site residues, remained virtually isomorphous to earlier crystal structures. Examination of the active site, however, indicated an unexpected result for substrate orientation. In contrast to the initial binding orientation employed by the theoretical model (*10*) (Figure 1), the electron density from the first data set shows that nicotine is oriented for coordination to occur between the pyridine nitrogen and the protein heme iron (Figure 2). Coordination is further supported by the continuous density between the nicotine pyridine and the heme. The distance between the nitrogen and the heme iron in the refined structure is 2.20 Å, while the cysteine 357 sulfur ligand is 2.30 Å from the iron. Another noteworthy feature of this model is the role of tyrosine 96. Recall that aforementioned mutagenesis studies and the molecular dynamics model indicate the importance of tyrosine 96 in substrate binding; however, tyrosine 96 is shown in the crystal structure to interact indirectly with the nonproductive orientation of nicotine by means of a water network between the tyrosine hydroxyl group and the pyrrolidine nitrogen of nicotine. One water molecule of this network acts as a hydrogen bond bridge between the pyrrolidine nitrogen and the tyrosine hydroxyl group. The other two water molecules in the active-site network have no obvious role, though their presence might be necessary for the positioning of the bridging water molecule. The contacts that nicotine makes with other atoms are shown in Figure 3. These observations led to the conclusion that nicotine initially binds in the manner of the previously studied inhibitors metyrapone and 1- and 4-phenylimidazole, which also bind by nitrogen coordination to the heme iron (*16*). This structure is available from the Protein Data Bank as structure 1P2Y.
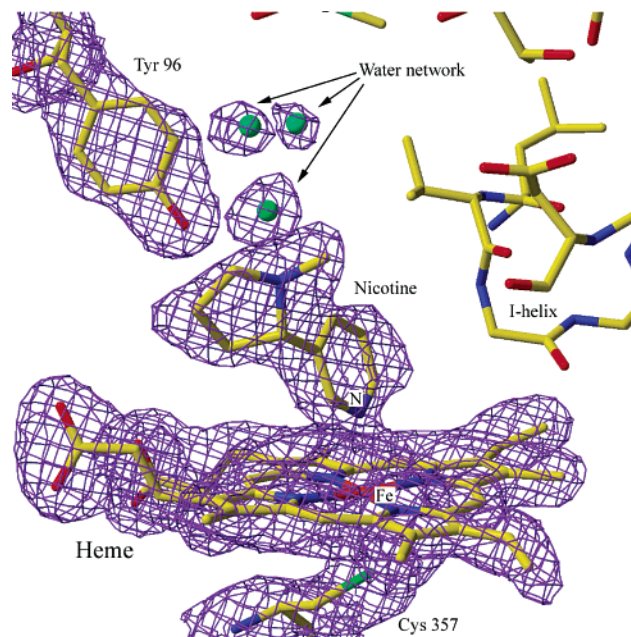

FIGURE 2: σA-weighted $2F_o - F_c$ omit map of the active site of the refined (*S*)-nicotine−P450cam complex. The map was computed at the 1σ level with the nicotine model omitted. Electron density contours have been omitted from some of the protein model for clarity.
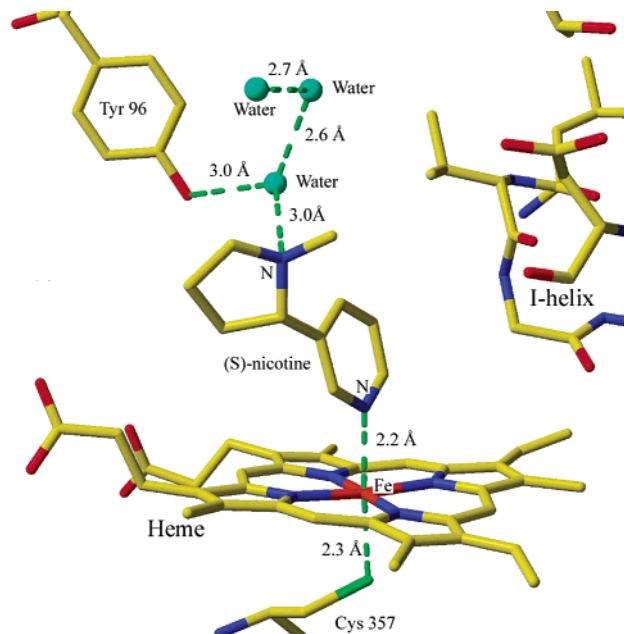

FIGURE 3: Active-site contacts for the nicotine−P450cam complex. The nicotine pyridine nitrogen is coordinated with the heme iron; one member of the water network acts as a hydrogen-bonding bridge between the tyrosine 96 hydroxyl group and the nicotine pyrrolidine nitrogen.

Data Set B: CO-Exposed Nicotine−P450cam Complex. The finding that nicotine is bound in an unproductive orientation suggested that a competing ligand might be required to displace the coordinated pyridine ring. Consequently, CO was introduced as described in the Experimental Methods section. The initial $F_o - F_c$ simulated annealing omit map from data set B showed an unambiguous change in the position of the nicotine molecule relative to that seen in the P450cam−nicotine structure (Figure 4A). Attempts were first made to account for the lobe of density near the
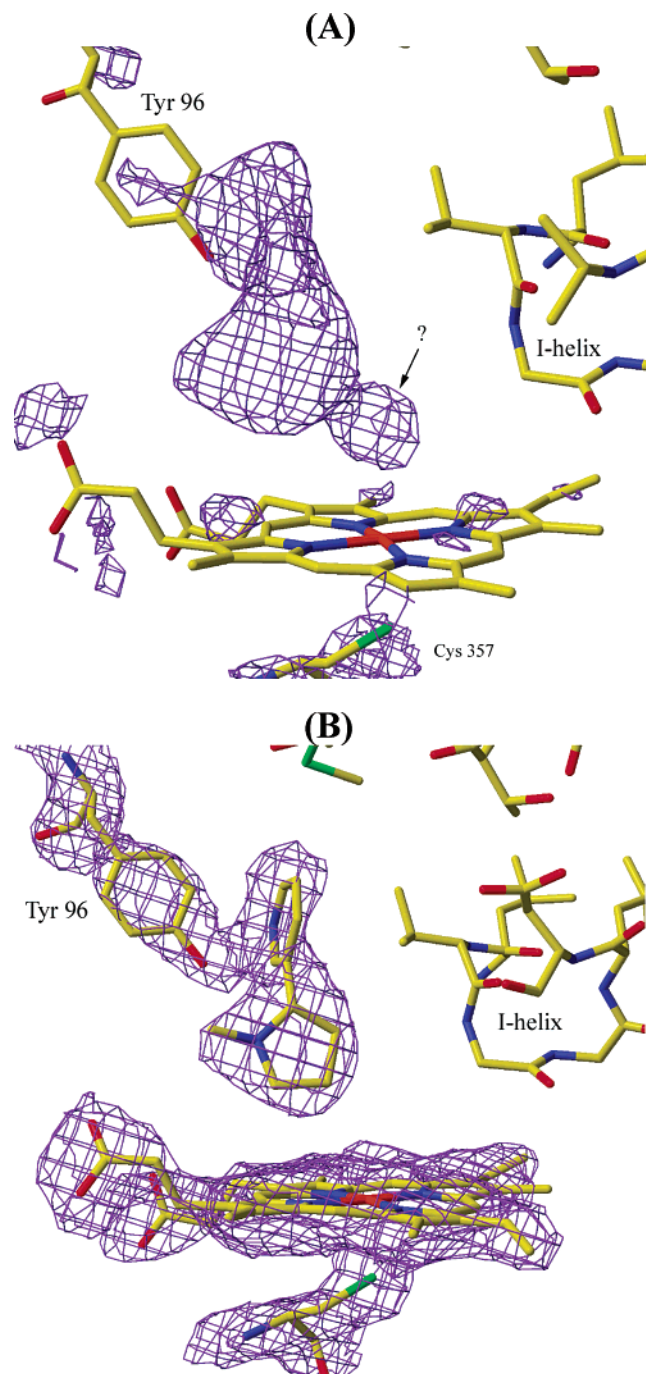
(A)

Tyr 96

I-helix

?

Cys 357

(B)

Tyr 96

I-helix

FIGURE 4: (A) σA-weighted $F_o - F_c$ Cartesian-simulated annealing omit map of the active site of the nicotine−P450cam complex following CO exposure. The map was computed at the 2σ level with a dummy nicotine model omitted. Electron density contouring has been removed from some of the protein model for clarity. Note the presence of the small density region near the heme iron. (B) σA-weighted $2F_o - F_c$ omit map of the active site of the refined nicotine−P450cam complex following CO exposure. The map was computed at the 1σ level with the nicotine model omitted. Electron density contouring has been removed from some of the protein model for clarity.

heme by presuming that either carbon monoxide or a water molecule was coordinated with the heme. However, the distance and position of the density peak are not consistent with a coordinated water molecule, as observed in the 2-phenylimidazole−P450cam complex (16), or with the water molecule or hydroxide anion seen as an axial heme ligand in the substrate-free P450cam crystal structure (14).
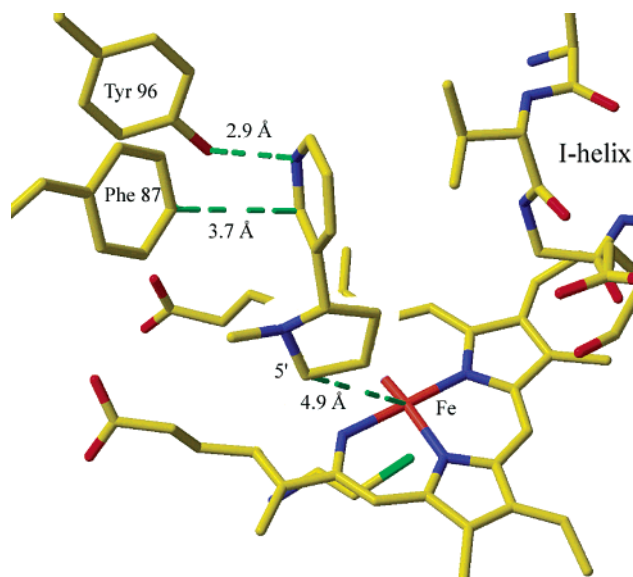

Tyr 96

2.9 Å

Phe 87

3.7 Å

I-helix

5'

4.9 Å   Fe

FIGURE 5: Active-site contacts for the nicotine−P450cam complex following CO exposure. The nicotine pyridine nitrogen is bonded to Tyr 96 rather than coordinated with the heme iron, rendering the 5' pyrrolidine accessible to hydroxylation. Phe 87 is also seen to make hydrophobic contact with the nicotine pyridine.

Similarly, the peak position is inconsistent with the carbon monoxide distance and geometry previously observed in the ternary complex of P450cam (17). This prompted refinement using partial occupancy models for the nicotine, as a means of addressing the possibility of multiple binding modes being present in the crystal. Although the crystallographic R values from structure refinement provided no way to discriminate among these models, the electron density was best fit by nicotine positioned entirely in the new uncoordinated orientation. A $2F_o - F_c$ omit map of this structure after refinement indicated that the unexplained density was absent at the 1σ level, while interaction between the nicotine pyridine and tyrosine 96 is clearly defined (Figure 4B). The contacts that the nicotine makes in the new orientation are summarized in Figure 5. This structure is available from the Protein Data Bank with the identifier 1P7R.

A positive pressure of carbon monoxide was not maintained during data collection, so the absence of binding-site carbon monoxide is not surprising. The results presented herein are consistent with a infrared spectroscopy study of carbon monoxide bound to P450cam (36). These measurements indicated that the rate constant k_{off} for CO dissociation, which is 0.3 s^{-1} at 240 K in the presence of (1R)-camphor, increases to 1.0 s^{-1} in the presence of (1S)-camphor. A correlation was made between more rapid dissociation of CO and the higher active-site mobility of (1S)-camphor, which has been crystallographically determined to have two binding modes (37). This argument would apply as well to (S)-nicotine. Thus, it is possible that it is not the binding of carbon monoxide that induces reorientation, but rather the reduction of the iron to Fe(II), or a combination of reduction and carbon monoxide binding.

DISCUSSION

Cytochrome P450 enzymes play a pivotal role in drug metabolism, and P450-related metabolic events are responsible for the failure of a number of compounds under

development (*38*). With the increase in three-dimensional structures for mammalian enzymes, it is important to understand the structural information that may be needed in drug design efforts. While many studies have been done on the bacterial P450 enzymes, our predictive ability based on these structures has been limited.

When a P450 substrate contains a nitrogen atom, the nitrogen forms a stronger bond to the ferric iron than does oxygen, resulting in an increase in the low-spin state and a red shift in the Soret band. The resulting ligand difference spectrum, that has a peak between 425 and 430 nm and trough between 390 and 410 nm, is a characteristic of type II binding. While (*S*)-nicotine gives a type II spectrum, it is not clear which nitrogen is coordinated to the heme iron. The pyrrolidine nitrogen is the most basic and could coordinate strongly, while the pyridine nitrogen is more accessible for coordination.

To test which binding mode is the most dominant for nicotine, we synthesized a nicotine analogue without nitrogen in the aromatic ring ((*S*)-*N*-methyl-2-phenylpyrrolidine). Since (*S*)-*N*-methyl-2-phenylpyrrolidine contains only one nitrogen atom (in the pyrrolidine ring), this must be the nitrogen coordinated to the heme iron. This compound did give a type II spectrum, so the pyrrolidine nitrogen can coordinate to the iron. However, nicotine binds 250 times more tightly than (*S*)-*N*-methyl-2-phenylpyrrolidine, with the only difference in structure being a nitrogen in the six-membered ring. The most obvious conclusion is that, while the pyrrolidine nitrogen can coordinate to the iron, it does not do so with a high affinity with nicotine binding via coordination through the pyridine nitrogen.

To test if this conclusion is correct, we determined the crystal structure of P450cam with nicotine bound. The results are shown in Figure 2, and indicate that the pyridine ring is coordinated to the iron when the heme is in the 3+ ferric state.

Thus, the crystal structure and binding spectra show that the major binding mode is most likely the result of coordination between the heme iron and the nicotine pyridine nitrogen (Figure 2). However, such an orientation does not allow for formation of the observed nicotine hydroxylation products (*20*). The active orientation might be crystallographically unobservable due to a very small number of the total binding events leading to product formation, and hence being overwhelmed in the crystal structure by the nonproductive mode. In solution, nicotine could also be displaced from the active site by molecular oxygen binding, only to rebind in a productive orientation. Alternatively, nicotine could reorient within the active site without complete dissociation from the enzyme. This hypothesis has parallels with a theoretical explanation for the binding of thiocamphor to P450cam, which displays an apparently nonproductive binding orientation in the crystal structure (*15*). Since tyrosine 96 is involved in stabilizing this nonproductive binding through a water atom intermediary, rebinding or reorientation would presumably be energetically unfavorable unless tyrosine 96 is also involved in a hydrogen bond in the productive binding mode, which is an assumption of the original theoretical model (Figure 1).

The first such experimental verification of significant substrate reorientation within the P450cam active site is provided by the reduced CO-exposed P450cam−nicotine

complex, which clearly shows that oxygen analogue binding or heme reduction to the ferrous state induces a substantial change in the substrate position (Figure 5). The possible energy penalty of such reorientation appears to be offset by maintenance of a hydrogen bond with tyrosine 96. In this case, the hydrogen bond is between tyrosine 96 and the nicotine pyridine nitrogen. Phenylalanine 87 is in hydrophobic contact with the nicotine pyridine ring. This residue has also been seen to be in hydrophobic contact with the pyridine ring in inhibitors metyrapone, the phenyl ring in 1- and 4-phenylimidazole, and the imidazole moiety in 2-phenylimidazole (*16*).

Some idea about the magnitude of the tyrosine 96−nicotine interaction can be obtained with the *N*-methyl-2-phenylpyrrolidine analogue of nicotine. The difference in the relative K_s values indicates that *N*-methyl-2-phenylpyrrolidine binds between 250 and 80 times less strongly than nicotine. Both substrates have type II interactions with the iron. However, the interaction for *N*-methyl-2-phenylpyrrolidine must be with the sterically hindered pyrrolidine nitrogen, while nicotine is most likely interacting with the iron through the less hindered pyridine nitrogen. Previous studies by Chiba et al. have shown that increasing steric bulk near the site of interaction leads to a decrease in type II interactions by between 48- and 156-fold for 2-methylimidazole-containing compounds compared to the imidazole analogue of the same compound (*40*). While the comparison is not perfect, it can be estimated that around half of the change in interaction energy is a result of steric crowding and decreased type II interactions. The remaining difference in binding energy is due to a lack of hydrogen-bonding interaction between the substrate and the tyrosine 96-coordinated water molecule. The results do indicate that even the weak type II interaction displayed by *N*-methyl-2-phenylpyrrolidine must be stronger than the possible hydrogen bond interactions of the pyrrolidine ring with tyrosine 96, since the molecule does not reorient to make this hydrogen bond.

From the findings above, it is apparent that tyrosine 96 is involved in the binding of nicotine in nonproductive as well as productive binding modes. This suggests that its role in stabilizing the productive orientation is not as significant as for camphor-like substrates. Rather, the behavior of nicotine displays characteristics of the binding behavior of metyrapone and phenylimidazole inhibitors (*16*). The nonaromatic pyrrolidine moiety, however, provides a target for hydroxylation once nicotine is oriented in a productive geometry. Since the reduced CO-exposed structure does show a pyridine N−tyrosine 96 interaction, the orientation of the nicotine in the theoretical model (Figure 1) appears feasible.

Thus, instead of displacing a coordinated water molecule and changing the heme iron from low-spin to high-spin, nicotine replaces the water molecule as an axial-coordinated ligand. Presumably it is the binding of molecular oxygen that then displaces nicotine from the heme iron, leaving it free to either reorient within the active site or rapidly leave the active site and rebind (Figure 6). Note that there is a difficulty with this model, as the shift to pentacoordinate iron makes possible the first electron reduction step. It is unclear how molecular oxygen would bind while the iron is still hexacoordinate. One possibility is that a small amount of enzyme is not coordinated at any given time, and that this fraction is reduced. This has been postulated for
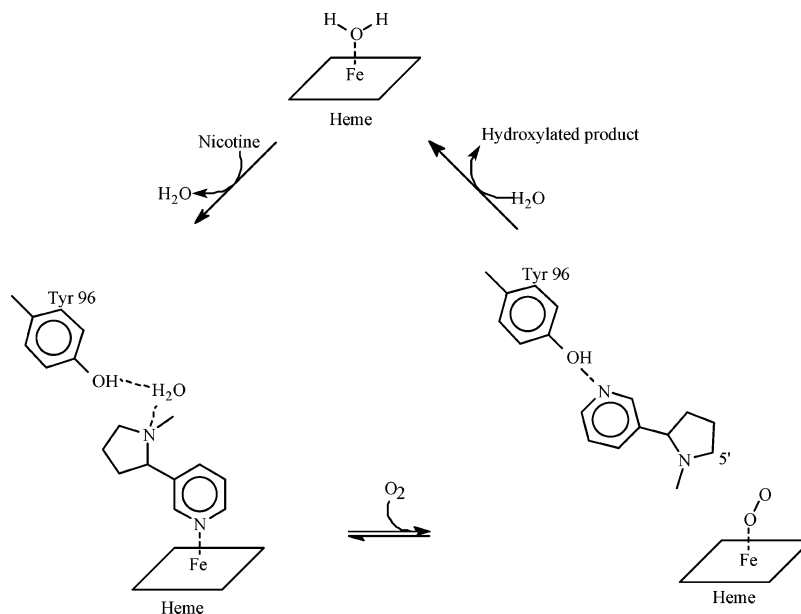
FIGURE 6: Hydroxylation of nicotine by P450cam, as inferred from crystallographic data. Note that the oxygen-binding step could either cause dissociation and rebinding of nicotine, or induce its reorientation within the active site.

roquefortine (*23*). The reduced form of the enzyme may have a lower affinity for nicotine, resulting in dissociation and oxygen binding. This same phenomenon is observed for HIV protease inhibitor and P4503A4 (*40*). In this case, comparison with structural analogues indicates that type II binding inhibits the rate of metabolism relative to that of compounds that do not coordinate to the iron, but these type II substrates still are metabolized.

Two possible reasons that could account for the failure of the previous MD studies to produce the correct orientation for initial substrate binding can be inferred from these studies. (1) The crystal structure indicates that at least one water molecule is associated with the pyrrolidine nitrogen when substrate is bound to the oxidized enzyme (Figure 3). Since the pyrrolidine nitrogen is the most basic, it is more likely to interact with a water molecule than the pyridine nitrogen, leaving the pyridine nitrogen free to form a type II interaction. Since no water was placed in the active site in the MD simulation, this would not have been modeled. (2) The parameters may overestimate the electrostatic interaction between the substrate nitrogens and the heme iron. Both nitrogen atoms on nicotine could be overestimated by about the same extent, leading to a strong electrostatic attraction at both the pyridine and pyrrolidine nitrogens. Since the pyrrolidine nitrogen has the highest negative charge, the orientation with pyrrolidine bound to iron would be preferred. Overestimation of the electrostatic attraction would overwhelm the steric clash between the hindered pyrrolidine ring nitrogen and the heme iron, leading to a prediction that this is the favored binding orientation. This is most likely a result of a too positive iron atom in the heme, given the low level of theory (UHF/LANL1MB) used in these calculations.

In conclusion, the results from the studies presented indicate that multiple structures for different oxidation states with substrate bound need to be obtained if predictions about regioselectivity and binding are to be made for the P450cam–nicotine complex. This is not unlike previous results obtained for another P450 enzyme, P450BM-3, which undergoes a substrate conformational change and major substrate motion after binding and upon reduction (*41*). These findings underscore the subtleties that are involved in successfully modeling enzyme−substrate interactions and the mobility that the P450cam active site offers for substrates. The data presented herein indicate that nicotine binds in a nonproductive orientation that would be the proper structure for predicting binding affinity and inhibitory capacity (Figure 6). The substrate then undergoes a large change in orientation that is apparently a result of oxygen binding to the iron or reduction of the enzyme (Figure 6). This orientation is the appropriate one for predicting regioselectivity and the kinetic features of substrate oxidation. While it is not clear that such complicated behavior will be exhibited for other enzyme−substrate interactions, it is clear that a single crystal structure for a given substrate−enzyme interaction may not provide a complete picture.

ACKNOWLEDGMENT

REFERENCES

1. Collins, J. R., and Loew, G. H. (1988) *J. Biol. Chem. 263*, 3164−3170.
2. Collins, J., Camper, D., and Loew, G. (1991) *J. Am. Chem. Soc. 113*, 2736−2743.
3. Ortiz de Montellano, P. R., Fruetel, J. A., Collins, J. R., Camper, D. L., and Loew, G. H. (1991) *J. Am. Chem. Soc. 113*, 3195−3196.
4. Chang, Y., Loew, G. H., Rettie, A. E., Baillie, T. A., Sheffels, P. R., and Ortiz de Montellano, P. R. (1993) *Int. J. Quantum Chem. Quantum Biol. Symp. 20*, 161−180.
5. Fruetel, J., Chang, Y., Collins, J., Loew, G., and Ortiz de Montellano, P. R. (1994) *J. Am. Chem. Soc. 116*, 11643−11648.
6. Harris, D., and Loew, G. H. (1995) *J. Am. Chem. Soc. 117*, 2738−2746.
7. Filipovic, D., Paulsen, M. D., Loida, P. J., Sligar, S. G., and Ornstein, R. L. (1992) *Biochem. Biophys. Res. Commun. 189*, 488−495.
8. Loida, P. J., Sligar, S. G., Paulsen, M. D., Arnold, G. E., and Ornstein, R. L. (1995) *J. Biol. Chem. 270*, 5326−5330.
9. Paulsen, M. D., Manchester, J., and Ornstein, R. L. (1996) *Methods Enzymol. 272*, 337−346.

10. Jones, J. P., Trager, W. F., and Carlson, T. J. (1993) *J. Am. Chem. Soc. 115*, 381−387.

11. Jones, J. P., Shou, M. G., and Korzekwa, K. R. (1995) *Biochemistry 34*, 6956−6961.

12. Cosme, J., and Johnson, E. F. (2000) *J. Biol. Chem. 275*, 2545−2553.

13. Williams, P. A., Cosme, J., Sridhar, V., Johnson, E. F., and McRee, D. E. (2000) *J. Inorg. Biochem. 81*, 183−190.

14. Poulos, T. L., Finzel, B. C., and Howard, A. J. (1987) *J. Mol. Biol. 195*, 687−700.

15. Raag, R., and Poulos, T. L. (1991) *Biochemistry 30*, 2674−2684.

16. Poulos, T. L., and Howard, A. J. (1987) *Biochemistry 26*, 8165−8174.

17. Raag, R., and Poulos, T. L. (1989) *Biochemistry 28*, 7586−7592.

18. Meuller, E. J., Loida, P. J., and Sligar, S. G. (1995) in *Cytochrome P450: Structure, Mechanism, and Biochemistry* (Ortiz de Montellano, P. R., Ed.) pp 83−124, Plenum Press, New York.

19. Ortiz de Montellano, P. R. (1995) *Cytochrome P450: Structure, Mechanism, and Biochemistry*, 2nd ed., Plenum: New York.

20. Carlson, T. J., Jones, J. P., Peterson, L., Castagnoli, N., Iyer, K. R., and Trager, W. F. (1995) *Drug Metab. Dispos. 23*, 749−756.

21. Peterson, L. A., and Castagnoli, N. (1988) *J. Med. Chem. 31*, 637−640.

22. Williams, D. E., Ding, X. X., and Coon, M. J. (1990) *Biochem. Biophys. Res. Commun. 166*, 945−952.

23. Aninat, C., Hayashi, Y., Andre, F., and Delaforge, M. (2001) *Chem. Res. Toxicol. 14*, 1259−1265.

24. Schlichting, I., Berendzen, J., Chu, K., Stock, A. M., Maves, S. A., Benson, D. E., Sweet, R. M., Ringe, D., Petsko, G. A., and Sligar, S. G. (2000) *Science 287*, 1615−1622.

25. French, K. J., Strickler, M. D., Rock, D. A., Rock, D. A., Bennett, G. A., Wahlstrom, J. L., Goldstein, B. M., and Jones, J. P. (2001) *Biochemistry 40*, 9532−9538.

26. Poulos, T. L., Perez, M., and Wagner, G. C. (1982) *J. Biol. Chem. 257*, 10427−10429.

27. Rodgers, D. W. (1994) *Structure 2*, 1135−1140.

28. Szebenyi, D. M. E., Arvai, A., Ealick, S., Laluppa, J. M., and Nielsen, C. (1997) *J. Synchrotron Radiat. 4*, 128−135.

29. Otwinowski, Z., and Minor, W. (1997) *Macromol. Crystallogr., Part A 276*, 307−326.

30. Brünger, A. T. (1992) *X-PLOR Version 3.1: A System for X-ray Crystallography and NMR*, Yale University Press, New Haven.

31. Pannu, N. S., and Read, R. J. (1996) *Acta Crystallogr., Sect. A 52*, 659−668.

32. Kleywegt, G. J., and Jones, T. A. (1995) *Structure 3*, 535−540.

33. McRee, D. E. (1999) *J. Struct. Biol. 125*, 156−165.

34. Matteson, D. S., and Kim, G. Y. (2002) *Org. Lett. 4*, 2153−2155.

35. French, K. J., Rock, D. A., Manchester, J. I., Goldstein, B. M., and Jones, J. P. (2002) *Arch. Biochem. Biophys. 398*, 188−197.

36. Contzen, J., Ristau, O., and Jung, C. (1996) *FEBS Lett. 383*, 13−17.

37. Schlichting, I., Jung, C., and Schulze, H. (1997) *FEBS Lett. 415*, 253−257.

38. Hodgson, J. (2001) *Nat. Biotechnol. 19*, 722−726.

39. Dean, J. A. (1985) *Lange's Handbook of Chemistry*, 13th ed., McGraw-Hill Books, New York.

40. Chiba, M., Jin, L., Neway, W., Vacca, J. P., Tata, J. R., Chapman, K., and Lin, J. H. (2001) *Drug Metab. Dispos. 29*, 1−3.

41. Oliver, C. F., Modi, S., Sutcliffe, M. J., Primrose, W. U., Lian, L. Y., and Roberts, G. C. (1997) *Biochemistry 36*, 1567−1572.